Available online at www.sciencedirect.com
ScienceDirect
Trans. Nonferrous Met. Soc. China 34(2024) 604−617
Transactions of Nonferrous Metals Society of China
www.tnmsc.cn

Microstructure and corrosion properties of Cu coatings deposited via laser-assisted low-pressure cold spray

Li-juan WU[1,2,3], Zhong-wei LIN[1,2,3], Zhun LUO[1,2,3], Bo LI[1,2,3], Jiang LIU[4], Qun-li ZHANG[1,2,3], Jian-hua YAO[1,2,3]

1. College of Mechanical Engineering, Zhejiang University of Technology, Hangzhou 310023, China;
2. Institute of Laser Advanced Manufacturing, Zhejiang University of Technology, Hangzhou 310023, China;
3. Collaborative Innovation Center of High-end Laser Manufacturing Equipment, Zhejiang University of Technology, Hangzhou 310023, China;
4. Zhejiang Reci Laser Technology Co., Ltd., Taizhou 317500, China

Received 31 August 2022; accepted 13 March 2023

Abstract: Cu coatings were prepared via the laser-assisted low-pressure cold spray (LPCS) method to study the effect of laser irradiation on microstructure and corrosion behaviors of the coatings. The results reveal that the laser-assisted LPCS-Cu coatings are denser and have better coating−substrate interfacial bonding as compared to LPCS-Cu coating. Laser irradiation improves the overall plastic deformation of deposited particles, resulting in uniform grain refinement of Cu particles. Therefore, the laser-assisted LPCS-Cu coatings show more uniform microstructure and smaller grain size. The results of electrochemical tests demonstrated that laser-assisted LPCS-Cu coatings have higher corrosion potential, lower corrosion current and corrosion rate than the LPCS-Cu coating in 3.5 wt.% NaCl solution. The main reason is that laser irradiation improves the coating density and intimate bonding between particles, and a continuous and dense corrosion product film composed of CuCl and Cu_2O is formed on the surface of the laser-assisted LPCS-Cu coating to block the erosion of the corrosive solution.

Key words: Cu coating; laser irradiation; cold spray; microstructure; corrosion properties

1 Introduction

Copper (Cu) and copper alloys have been widely used as protective coatings or components of seawater systems due to their good resistance to corrosion and biofouling as well as many other excellent properties [1,2]. Meanwhile, Cu is also a material with high thermal conductivity and is very sensitive to oxidation. Thus, it is very difficult to fabricate satisfied Cu coating through surface modification techniques with high heat-input such as laser cladding and thermal spraying [3−5].

Cold spraying (CS) is an emerging material deposition technology and has attracted widespread attention in the past 30 years because of its unique deposition behavior [6−8]. In CS process, micro-sized metallic particles are accelerated to supersonic velocity through a da-Laval nozzle and then impact, deform and adhere to a substrate or as-deposited particles, forming a coating [9]. During this process, the particles undergo extensive plastic deformation to achieve a firm bonding with the underlying material at a temperature well below the melting point [10]. Oxidation, phase transformation, residual tensile stress and other typical defects related to high-temperature deposition processes can thus be avoided in CS process. Therefore, these features of CS make it very suitable for the effective deposition of pure Cu and its alloys [11].

Corresponding author: Bo LI, Tel: +86-15088688625, E-mail: libo1011@zjut.edu.cn
DOI: 10.1016/S1003-6326(23)66421-0

The CS technique is usually classified into low-pressure CS (LPCS) and high-pressure CS (HPCS), which generally operate at pressures in the range of 0.5−1 MPa and 1−6 MPa, respectively [6,9]. The LPCS is commonly used in the field of repair because of its safe, portable, and low-cost features as compared to HPCS [9,12,13]. However, due to relatively low pressure and pre-heating temperature of carrier gas used in LPCS, the particle velocity in LPCS is much lower than that in HPCS, which would easily lead to the formation of pores in the coating because of insufficient plastic deformation of deposited particles. To eliminate this problem, ceramic shot-peening particles such as Al_2O_3, SiC, and B_4C, are employed to mix with the metal matrix to increase the plastic deformation of the metal matrix particles and thus decrease the coating porosity [14−16]. However, there is a high chance that ceramic particles would embed into the metal matrix and remain in the coating, which would change the composition and properties of the original metal matrix. In addition, hard ceramic particles would also erode the inner wall of the nozzle, thereby shortening its service life and affecting the operation of the equipment [17].

As a heat source with high energy density, laser has been introduced into CS process recently, which is named laser-assisted CS or supersonic laser deposition [18−20]. In such a process, the laser is used to synchronously heat both the substrate and the particles. The heating by laser simultaneously softens both the deposition site on the substrate and the spraying particles, the strength of which can be significantly reduced. Therefore, the formation of a coating can be fulfilled at impact velocities about half of that in CS [21]. In other words, with the assistance of synchronous laser heating, lower spraying parameters can be used to achieve identical coating quality by conventional CS with higher spraying parameters. It is expected that a dense metal coating can be obtained by laser-assisted LPCS without the addition of ceramic particles into the metal matrix. Although considerable research efforts have been devoted to investigating the effects of laser irradiation on the microstructure and properties of coatings deposited by HPCS process [22−24], there is a lack of studies concerning the influence of laser heating on LPCS deposits. Therefore, in this work the effect of synchronous laser heating on the characteristics and properties of LPCS-Cu coatings was studied. The microstructures and corrosion properties of LPCS-Cu coatings assisted with different laser irradiation powers were characterized and compared.

2 Experimental

2.1 Feedstock materials

Commercially available powders of electrolytic Cu with a purity of 99.97% (supplied by Zhongke Yannuo Technology Co., Ltd., China) were used as a coating material in this study. The morphology and particle size distribution of Cu powder are shown in Fig. 1. The particle shape of Cu powders was dendritic. Particle size distribution of the Cu powder

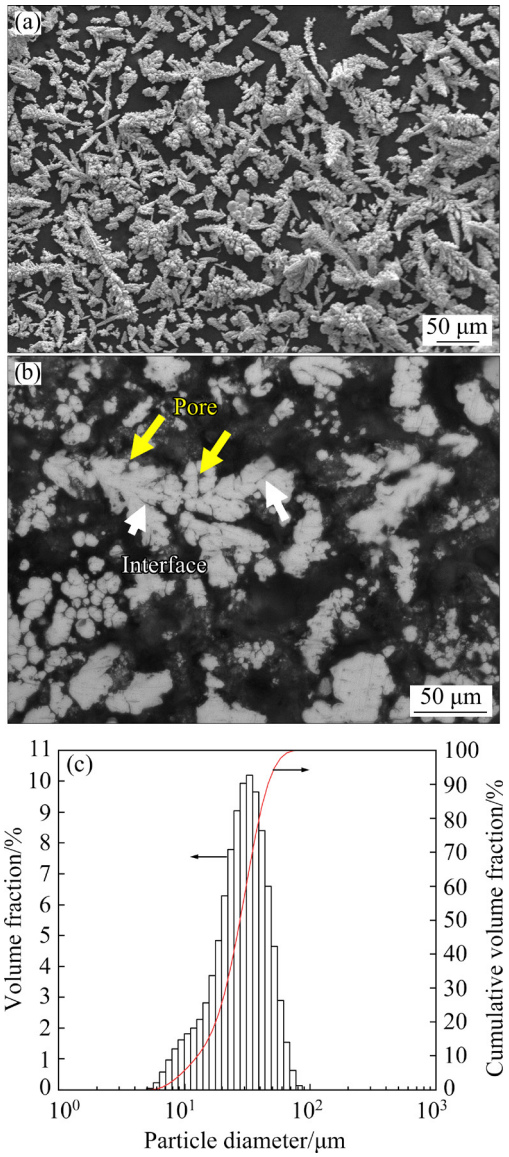

Fig. 1 Morphology (a), internal microstructure (b) and particle size distribution (c) of Cu powders

was measured by a laser diffraction particle size analyzer (Horiba LA−950, Japan), as shown in Fig. 1(c), indicating that the average particle sizes (D_{50}) of the Cu powders were 27.68 μm. Before spraying, the powders were dried for 2 h at 100 °C to improve their flowability. The substrate used was a pure Cu plate with dimensions of 100 mm × 50 mm × 5 mm. The substrates were cleaned with alcohol and then grit-blasted using Al_2O_3 particles (about 70 μm) before being coated. The measurement roughness of the substrate was R_a=(5.46±0.31) μm.

2.2 Coating fabrication

The Cu coatings were manufactured using a laser-assisted LPCS system mainly containing LPCS unit, laser unit, movement unit and gas supply unit. The schematic diagram of the system is shown in Fig. 2. The portable DYMET 423 system provided by DYCOMET Corporation was used as the LPCS unit. The converging-diverging Laval nozzle had a round cross-sectional shape with a diverging length of 130 mm and an expansion ratio of 1.275. The liquid nitrogen station with a compressor for gas pressure regulation provided compressed nitrogen as propellant gas. The feedstock powder was mixed with the nitrogen at the downstream of the nozzle and then accelerated and finally impinged onto the surface of the substrate which was synchronously heated by a fiber coupled diode laser (Laserline LDF6000−100 VGP, Germany) with a wavelength of 960−980 nm. The laser beam was round and the diameter of the laser spot was about 5 mm. The LPCS nozzle and laser head were assembled on a six-axis industrial robot (STAÜBLI TX 200L, Pfaeffikon, Switzerland) and moved together during the spraying process so that the area underneath the nozzle was always irradiated. The nozzle was perpendicular to the substrate surface while the laser beam was at an angle of approximately 30° to the surface normal. The spray parameters are listed in Table 1. The LPCS process parameters were optimized prior to the final spraying process. The laser power was adjusted to prepare different coatings to investigate the influence of laser irradiation on the microstructure and properties of the coatings. The coating was obtained by depositing one layer with a coating thickness of 700−800 μm.

2.3 Characterization of powders and coatings

The microstructures of the powders, as well as the coatings, were analyzed by optical microscopy (OM, Axio Scope. A1, Zeiss) and scanning electron microscopy (SEM, ΣIGMA HV−01−043, Carl Zeiss). The porosity of the coatings was calculated using image analysis (Image J) and ten optical micrographs with 500× magnification were used to determine the porosity of each coating. The deformation and size of grains in the coating were

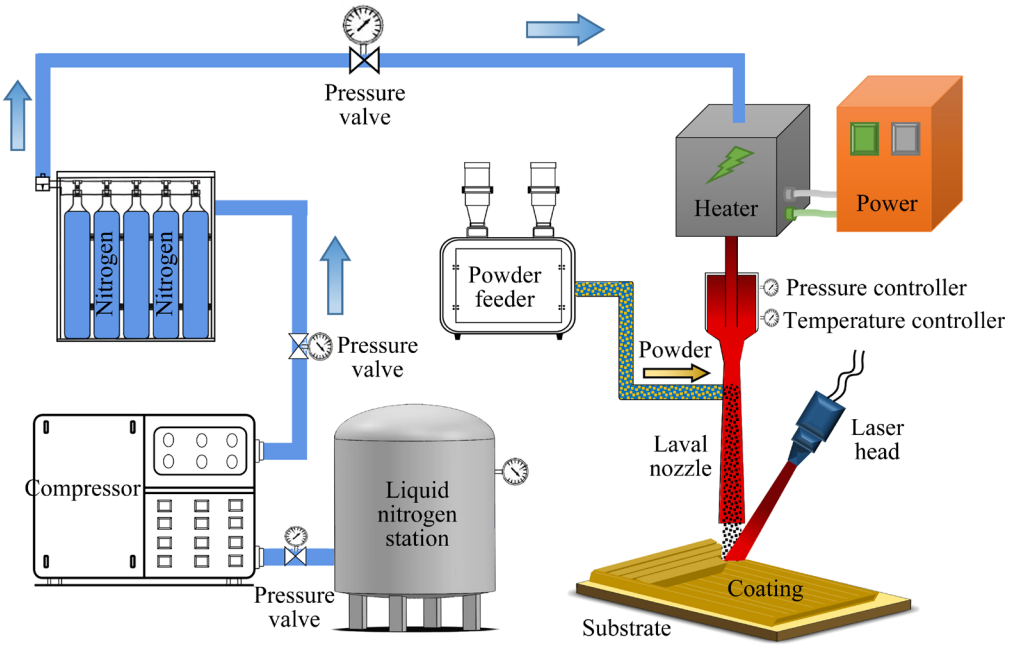

Fig. 2 Schematic diagram of laser-assisted LPCS system

Table 1 Process parameters for depositing Cu powder by laser-assisted LPCS

Parameter	Value
Propellant gas	Nitrogen
Gas pressure/MPa	0.8
Gas temperature/°C	400
Nozzle traverse speed/(mm·s^{-1})	10
Standoff distance/mm	15
Powder feed rate/(g·min^{-1})	12
Scan step/mm	2
Laser power/W	0, 500, 600, 700

characterized by a field emission scanning electron microscopy (Zeiss Gemini 500) equipped with electron backscattered diffraction (EBSD, OXFORD C-Nano). To prepare the EBSD analysis sample, mechanical grinding and polishing were conducted, then Ar ion beam bombardment (Fischione 1061) for 4 h was also used. The area for EBSD measurement was scanned with a step size of 100 nm and the software of Channel 5 was used for post-processing. After corrosion tests, the microstructures and element distribution of the corroded surfaces and cross-sections were analyzed by SEM and energy dispersive spectroscopy (EDS, Nano Xflash Detector 5010, Bruker) after corrosion tests. X-ray diffraction (XRD, Rigaku Ultima IV) analysis was used to determine the corrosion products. Measurements were carried out within the 2θ range from 10° to 100° with a step size of 0.02° and a scan rate of 5 (°)/min under Cu K_α radiation (λ=0.1541 Å).

2.4 Electrochemical measurements

The electrochemical test was implemented to evaluate the corrosion resistance of the coatings and substrate using an electrochemical workstation (CHI660D, Shanghai Chenhua Instrument Co., Ltd., China). A conventional three-electrode system was used as the electrochemical cell. The samples with an exposed area of 1.0 cm^2 to the solution were used as the working electrode. A platinum foil and the saturated calomel electrode (SCE) were served as the auxiliary and reference electrodes, respectively. Before the tests, the open circuit potential (φ_{OCP}) measurements for the samples were carried out in the solution of 3.5 wt.% NaCl at 25 °C. The φ_{OCP} was continuously monitored during 1000 s exposure. The electrochemical impedance spectroscopy (EIS) test was performed in a frequency range of 10^{-2}−10^5 Hz and a voltage amplitude of 5 mV. Afterwards, potentiodynamic polarization tests were conducted in the potential range from −0.5 to 0.5 V (vs OCP) at a scan rate of 1 mV/s. The corrosion potential (φ_{corr}) and corrosion current density (J_{corr}) were obtained by fitting the polarization curve based on Tafel extrapolation with CHI660E software [25]. The electrical equivalent circuit (EEC) was obtained by ZSimpwin software based on the EIS data.

3 Results and discussion

3.1 Microstructures of powder and coatings

Figure 1 shows the morphology and internal microstructure of the Cu powders. Many researchers have demonstrated that spraying powders with fine, irregular morphology and porous microstructure can be more easily accelerated than spherical particles during the LPCS process [26−28]. As shown in Fig. 1(b), there are apparent pores in the interior of particles, which probably increase the porosity of the deposited coating.

The low magnification optical micrographs of the laser-assisted LPCS-Cu coatings are shown in Fig. 3. All Cu coatings have a minimum thickness of 600 μm. It can be clearly seen that there is a gap between the coating and substrate, as shown in Fig. 3(a). Due to the low pressure and without reinforcement particles, the plastic deformation of some deposited particles and the matrix is insufficient to form a firm bond, resulting in the generation of gaps that easily lead to delamination between coating and substrate. However, it is found that the bonding between coating and substrate is very dense under laser irradiation as seen from Figs. 3(b)−(d). This may be due to the softened Cu particles and the surface of the substrate by laser heating, which can increase their plastic deformation ability and thus improve the interfacial bonding between coating and substrate. It was found by other researchers that preheating the particles and substrate can improve the bonding of the coating [29,30].

The cross-sectional microstructures of LPCS-Cu coatings produced with different laser irradiation powers are displayed in Fig. 4. Significant gaps can

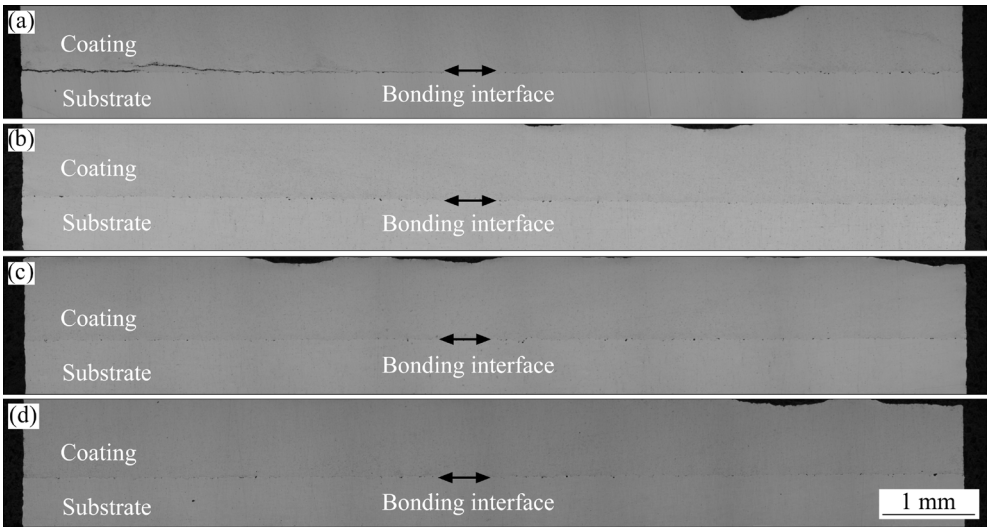

Fig. 3 Low magnification optical micrographs of LPCS-Cu coatings assisted with different laser powers of 0 W (a), 500 W (b), 600 W (c), and 700 W (d)

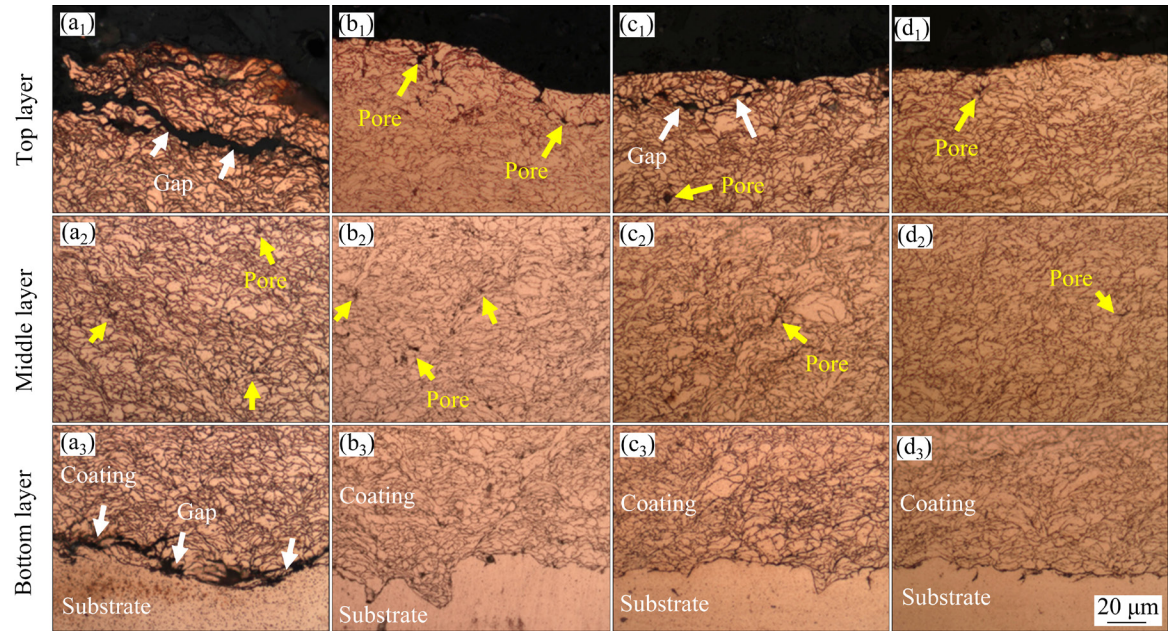

Fig. 4 Cross-sectional microstructures of LPCS-Cu coatings assisted with different laser powers of 0 W (a_1−a_3), 500 W (b_1−b_3), 600 W (c_1−c_3), and 700 W (d_1−d_3)

be detected at the top of the LPCS-Cu coating, as shown in Fig. 4(a_1), which are mainly attributed to the insufficient plastic deformation of the sprayed particles during deposition, suggesting relatively poor inter-particle bonding. As reported previously [31,32], the top surface layer of the CS coating was relatively porous as compared to the bottom layer, resulting from a tamping effect of the bottom layer by the stream of Cu particles. Compared to the LPCS-Cu coating, the top microstructures of Cu coatings become denser when laser irradiation is applied. The particles more easily deform during the deposition process because of the heating and softening effect of laser irradiation.

There are a large number of interfaces in the coatings, as shown in Fig. 4, which consist of two types of particle−particle interface and multibranched interface of the dendritic particle, as indicated by the white arrows in Fig. 1(b). Due to the existence of multibranched interface of the dendritic particle, the deformation of particles becomes complicated, and it is difficult to observe

the plastic deformation of individual particle clearly. It can also be observed that there are a small number of pores at the triple particle junctions inside all coatings, which is an unavoidable problem in the LPCS process. Porosity is one of the critical indicators to evaluate the quality of cold sprayed layers, which is mainly reflected in the bond between particles and is related to the deformation degree of particles. In CS coatings, the gaps between poorly bonded particles usually act as the fast pathway for the corrosive media to penetrate into the coating. The in-depth penetration rate of the corrosive media is determined by the number of connected inter-particle gaps or pores [33]. The coating porosity of different samples was measured to analyze and evaluate the effect of the laser irradiation power on the deposition quality of LPCS-Cu coatings. The porosity of laser-assisted LPCS-Cu coatings with laser power of 0, 500, 600, and 700 W is (2.22±0.47)%, (1.86±0.42)%, (1.63±0.39)%, and (1.00±0.26)%, respectively. This shows that the introduction of laser into the LPCS process improves the densities of the Cu coatings. With the increase of laser irradiation power, the porosity of the coating decreases. KOIVULUOTO et al [34] also reported similar results in laser-assisted cold-sprayed Al coatings. Laser irradiation can enhance the plastic deformation ability of Cu particles, and the softened particles are more fully deformed and easier to combine during the deposition process. However, the possibility of high-temperature oxidation of copper will increase when the laser irradiation power is too high. Therefore, it is necessary to control the laser irradiation power within a reasonable range, which can effectively improve the deposition quality and improve the compactness of the coating.

3.2 EBSD characterization of coatings

Figure 5 shows the EBSD image quality (IQ) and inverse pole figure (IPF) maps of LPCS-Cu coatings assisted with different laser irradiation powers. The impact direction of the particles is parallel to the *Y* axial coordinate. As shown in Fig. 5(a_1), there are more low or un-indexed regions (highlighted by arrows) in the LPCS-Cu coating, which indicates weak bonding, high defect density, or lattice strain in the interfacial regions [35]. Besides, two very different grain sizes are observed in the coating, presenting inhomogeneous deformation. The average grain size of the LPCS-Cu coating is 0.588 μm. In contrast, the laser-assisted LPCS-Cu coatings have lower fractions of low or un-indexed regions, indicating a progressive reduction of particle boundary defects and improved interfacial bonding. Figures 5(b_1) and (c_1) clearly show the deformation of the particles with high dislocation density at the boundaries. The particle deformation upon impact is mainly limited to the immediate vicinity of the particle boundaries, resulting in grain refinement, while the central regions of the particles undergo much less deformation, thus preserving coarser grains [36]. The typical bimodal grain size distribution for CS coating with larger grains in the interior of the spray splats surrounded by fine-grained areas at the inter-particle interfaces is observed in Figs. 5(b_2) and (c_2). Furthermore, as seen from Figs. 5(d_1) and (d_2), the IQ image of the LPCS-Cu coating with the assistance of 700 W laser power shows a uniform brightness pattern, overall deformation of particles, and grain size. A more uniform structure with a smaller average grain size (0.289 μm) was obtained at 700 W laser-assisted LPCS-Cu coating as compared to the counterpart without laser assistance. Therefore, it can be concluded that laser irradiation leads to greater plastic deformation of the particle and thus more uniform structure of the coating. In addition, most of the grains in all coatings show a rather wide spread of orientations and the coatings show no texture.

3.3 Corrosion test

3.3.1 Electrochemical properties

The open circuit potential (φ_{ocp}) evolution of the Cu coatings in 3.5 wt.% NaCl solution is depicted in Fig. 6(a). All φ_{ocp} curves could be analyzed by dividing them into three stages. In the first stage, the φ_{ocp} value increases, which could be attributed to the formation of the passive film on the surface. In the second stage, the φ_{ocp} value decreases, which represents the dissolution of the native oxide film. After a long time of immersion, the φ_{ocp} value is gradually stabilized, indicating a dynamic balance between the formation and dissolution of the passive layers.

Potentiodynamic polarization curves of the Cu coatings generated by the electrochemical tests carried out in 3.5 wt.% NaCl solution are reported

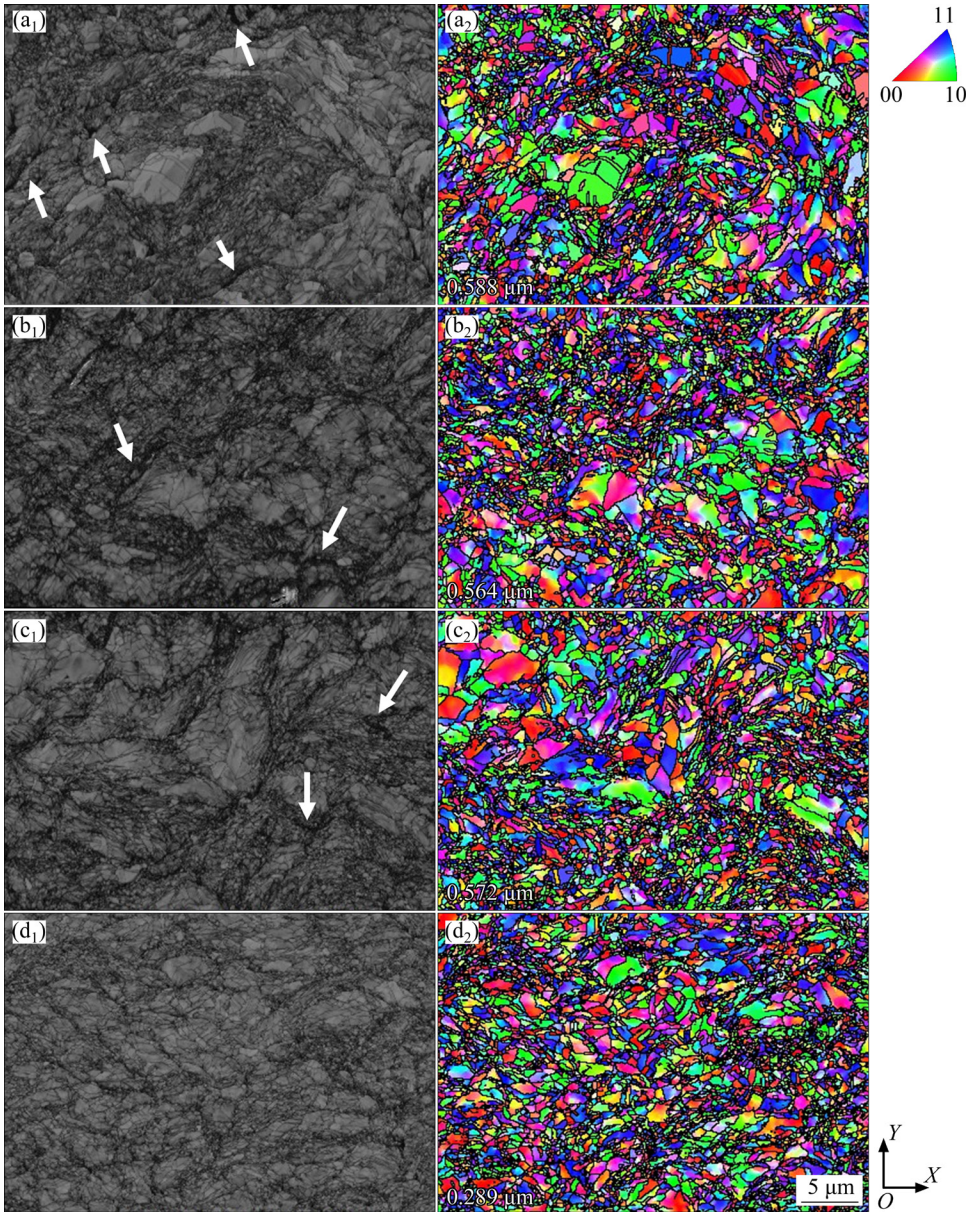

Fig. 5 EBSD image quality (IQ) (a_1, b_1, c_1, d_1) and inverse pole figure (IPF) (a_2, b_2, c_2, d_2) maps of laser-assisted LPCS-Cu coatings with different laser powers of 0 W (a_1, a_2), 500 W (b_1, b_2), 600 W (c_1, c_2), and 700 W (d_1, d_2)

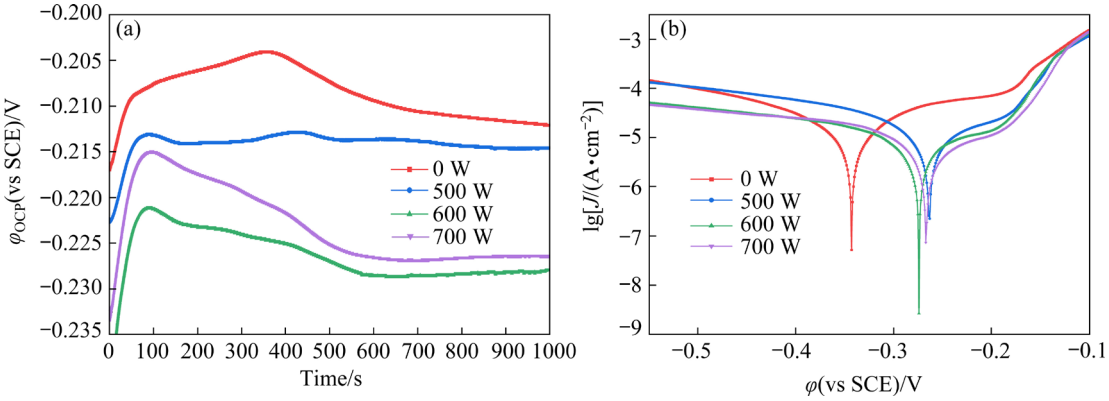

Fig. 6 Open circuit potential versus time profile (a) and potentiodynamic polarization curve (b) of LPCS-Cu coatings assisted with different laser powers

in Fig. 6(b). As can be seen from the curves of the samples, there are some differences in corrosion potentials and corrosion current density of the LPCS-Cu coating assisted with different laser powers. The corrosion potential (φ_{corr}) and corrosion current density (J_{corr}) obtained from polarization curves are summarized in Table 2. These parameters are used to characterize the corrosion resistance of Cu coatings [37]. As shown in Table 2, the φ_{corr} values of the LPCS-Cu coatings with laser powers of 500, 600, and 700 W are −0.263, −0.274, and −0.267 mV, respectively, while that of LPCS coating without laser irradiation is −0.343 mV. A more positive φ_{corr} value means that the sample has higher chemical stability under the corrosive environment. The corrosion potential of the laser-assisted LPCS-Cu coatings shifts towards more noble values as compared to that of the LPCS-Cu coating, which means that the laser-assisted LPCS-Cu coatings have a lower anodic reaction rate. Subsequently, the J_{corr} is a critical parameter commonly used to further evaluate the reaction kinetics of corrosion. It is almost directly used to characterize the corrosion rate at φ_{corr}. The J_{corr} value of the LPCS-Cu coating without laser irradiation is 3.093×10^{-5} A/cm^2, which is higher than that of the laser-assisted LPCS-Cu coatings. The lower J_{corr} value and higher φ_{corr} value indicate that laser-assisted LPCS-Cu coatings have good corrosion resistance. The poor corrosion performance of LPCS-Cu coating can be attributed to the decrease in compactness of the coating structure.

Table 2 Results of potentiodynamic polarization test of LPCS-Cu coatings assisted with different laser irradiation powers

Laser power/W	φ_{corr} (vs SCE)/V	J_{corr}/(A·cm^{-2})
0	−0.343	3.093×10^{-5}
500	−0.263	1.786×10^{-5}
600	−0.274	1.448×10^{-5}
700	−0.267	1.260×10^{-5}

To further understand the corrosion resistance of the coatings, the EIS was measured. Figure 7 shows the evolution of Nyquist and Bode plots of the laser-assisted Cu coatings in a 3.5 wt.% NaCl solution. The solid fitting lines are plotted according to the equivalent circuit shown in Fig. 7(a). The

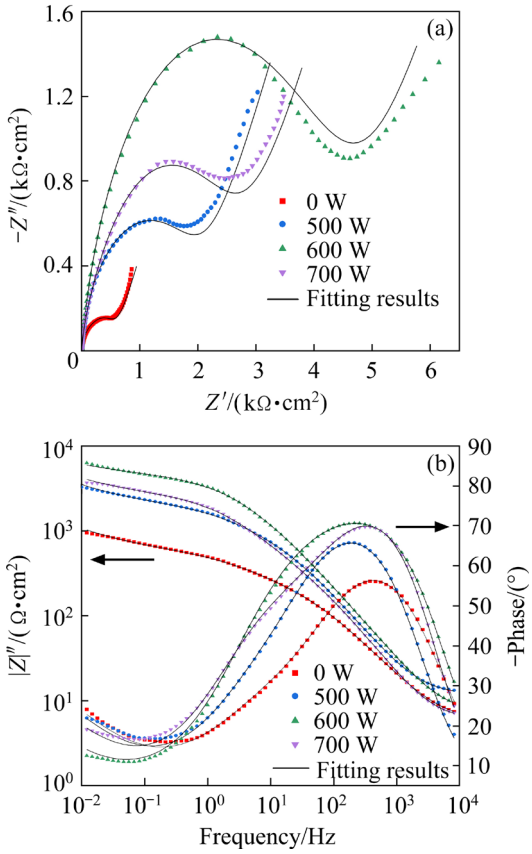

Fig. 7 Nyquist (a) and Bode (b) plots of laser-assisted LPCS-Cu coatings with different laser powers in 3.5 wt.% NaCl solution

Nyquist plots exhibit two capacitive loops, presented in the high frequency area and low frequency area, respectively. Capacitive semi-circle at high frequency is related to the formation of corrosion products, whereas low frequency is related to the double-electric layer. Larger capacitive loop diameters mean higher impedance, indicating the effect of the corrosion product film on inhibiting corrosion. All the coatings present similar Nyquist and Bode plots, suggesting the same corrosion reaction occurred on the Cu coating side. However, the laser-assisted LPCS-Cu coatings exhibit larger sizes of semi-circle loops than the LPCS-Cu coating, in which the capacitive arc radius of the sample with 600 W laser power is the largest. Besides, from the Bode plot shown in Fig. 7(b), it can be seen that laser-assisted LPCS-Cu coatings have the higher impedance modulus and LPCS-Cu coating has the lowest impedance modulus, which indicates that the corrosion product films on the surface of Cu coatings are dense and have good corrosion inhibition protection.

Based on the impedance plot, the EEC of the Cu coatings can be described in Fig. 8. In this way, R_s is the solution resistance, R_{ct} is the charge transfer resistance, Q_p and Q_{dl} are the constant phase element (CPE) for the porous and dense layers, respectively, include two components of Q–T (the frequency-independent admittance) and Q–n (the dispersion index), R_p is the local corrosion resistance, and Z_w is the diffusion impedance. From the modeled ECC, the fitted impedance spectra are represented in Table 3, where the chi-squared (χ^2) is the fitting error. It can be noted that the laser-assisted LPCS-Cu coating with 600 W exhibited the highest R_{ct} value, while the LPCS-Cu has the lowest R_{ct} value. It is widely known that the R_{ct} is an important parameter that directly represents the corrosion rate of the sample. In general, the greater the R_{ct} value is, the lower the corrosion rate [38]. The R_{ct} values for the laser-assisted LPCS-Cu coatings with laser powers of 500, 600, and 700 W are 1371, 4326, and 2430 Ω/cm^2, respectively, while that of LPCS-Cu coating is 422.7 Ω/cm^2. It can be easily found that the synchrotron irradiation of the laser can significantly increase the R_{ct} of the LPCS-Cu coating and improve the corrosion resistance, mainly due to fewer defects in the coating. The previous studies show that decreasing the porosity and cracks will improve the corrosion protection of cold-sprayed coating [39]. Therefore, the lowest porosity of the Cu coatings prepared by laser-assisted LPCS would be the reason for excellent corrosion performance. However, corrosion performance of laser-assisted LPCS-Cu coatings declined when the laser power was from 600 to 700 W. The decline was attributed to a higher degree of plastic deformation at higher laser powers, changing the chemical potential of the metal atoms in the deformed area and leading to more active sites for corrosion [40,41].

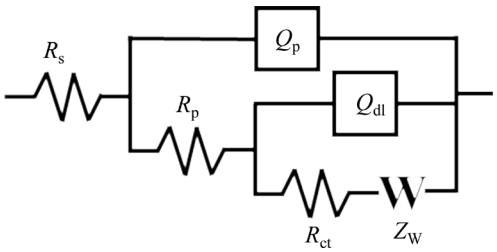

Fig. 8 Equivalent circuit model for Cu coatings

3.3.2 Characterization of corrosion products

Figure 9 presents the surface morphologies of the laser-assisted LPCS-Cu coatings after corrosion test. It can be observed that uniform corrosion appears on the surface of the sample corroded in 3.5 wt.% NaCl solution and corrosion products are formed. It can be seen from Figs. 9(a)−(d) that the corrosion products increase at first and then decrease with the increase of laser power, and the corrosion products of LPCS-Cu coating are the least. As seen from Figs. 9(a) and (a$_1$), the LPCS-Cu coating presents a smoother surface and fewer pits, which shows lower corrosion sensitivity. Compared with LPCS-Cu, a large number of corrosion products are observed on the surface of laser-assisted LPCS-Cu coatings, as shown in Figs. 9(b)−(d). In addition, the cubic particles (marked by dashed line ellipses in Figs. 9(b$_1$) and (c$_1$)) are observed distinctly on the corroded surface of the 500 and 600 W laser-assisted LPCS-Cu coatings. The Cu and Cl elements in cubic particles were detected by the EDS analysis, and the molar ratio of the two elements is approximately 1:1, as shown in Figs. 10(a) and (b). The cubic particles are identified as CuCl particles according to the morphology and EDS analysis of the particles [42].

EDS analysis revealed that the corrosion products on the coating surface mainly consisted of Cu, Cl and O, as reported in Fig. 10. In order to identify the corrosion products characteristics after

Table 3 Various electrical parameters obtained after equivalent circuit fitting of EIS data for LPCS-Cu coatings assisted with different laser powers

Laser power/W	R/ (Ω·cm^2)	Q_p−T/ (F·cm^{-2})	Q_p−n	R_p/ (Ω·cm^2)	Q_{dl}−T/ (F·cm^{-2})	Q_{dl}−n	R_{ct}/ (Ω·cm^2)	Z_w/ (Ω·cm^2·s$^{-0.5}$)	χ^2
0	5.549	4.727×10^{-5}	0.8032	206.2	4.707×10^{-4}	0.5882	4.227×10^{2}	6.433×10^{-3}	3.872×10^{-4}
500	1.164	2.013×10^{-5}	0.8718	765.6	1.454×10^{-4}	0.6047	1.371×10^{3}	2.093×10^{-3}	5.013×10^{-4}
600	7.066	1.487×10^{-5}	0.8787	619.7	4.969×10^{-5}	0.4796	4.326×10^{3}	2.006×10^{-3}	3.409×10^{-4}
700	6.051	1.528×10^{-5}	0.9209	362.2	8.601×10^{-5}	0.6204	2.430×10^{3}	2.054×10^{-3}	4.486×10^{-4}

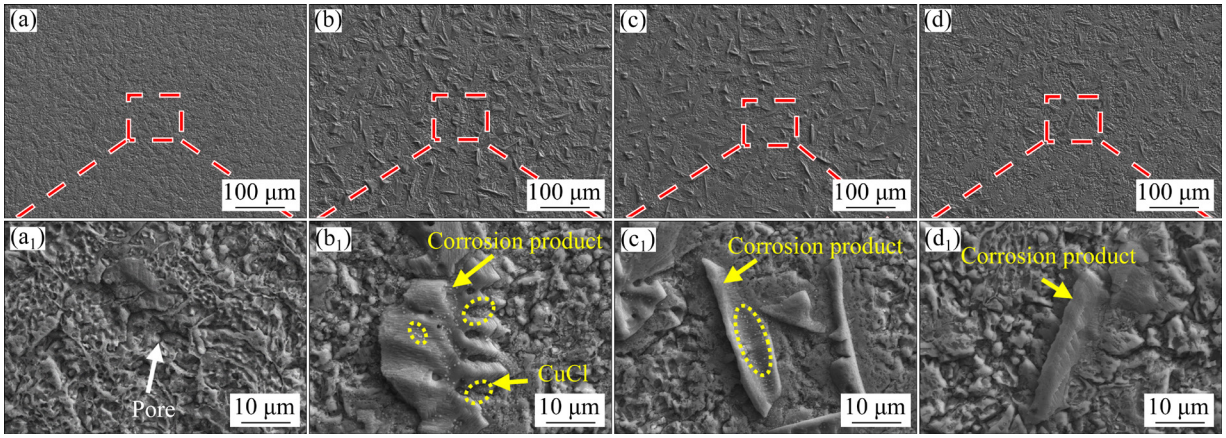

Fig. 9 Surface corrosion morphologies of LPCS-Cu coatings assisted with different laser powers after corrosion in 3.5 wt.% NaCl solution: (a, a_1) 0 W; (b, b_1) 500 W; (c, c_1) 600 W; (d, d_1) 700 W

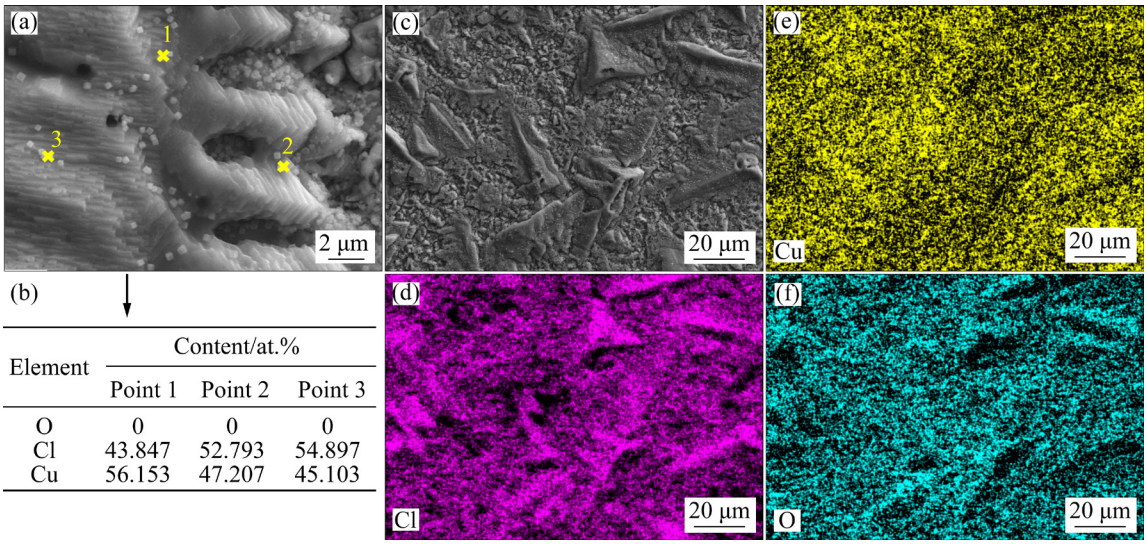

Element	Content/at.%		
	Point 1	Point 2	Point 3
O	0	0	0
Cl	43.847	52.793	54.897
Cu	56.153	47.207	45.103

Fig. 10 EDS results of corrosion products

anodic polarization measurements, XRD analysis was used and the patterns of the samples are shown in Fig. 11. By calibrating the characteristic peaks, it is found that the corrosion product of the four samples is mainly composed of Cu_2O and CuCl. It is generally accepted that corrosion of Cu in neutral NaCl solutions takes place with the chlorination and oxidation reaction of the Cu [15,32,43]. Surfaces were ultimately covered by the oxide and chloride forms of the Cu.

Figure 12 shows the cross-sectional microstructure and EDS results of laser-assisted LPCS-Cu coatings after corrosion in 3.5 wt.% NaCl solution. The corrosion product film produced on the surface of LPCS-Cu coating is less and not continuous, while that of laser-assisted LPCS-Cu coatings has a certain thickness and is relatively

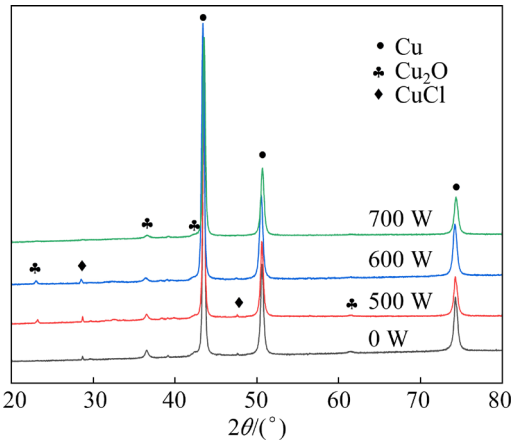

Fig. 11 XRD patterns of Cu coatings after corrosion test

continuous, which can be confirmed by the distribution of Cl element in Fig. 12. The continuous corrosion products form a protective

film on the surface of the coating, reducing the corrosion rate. Moreover, the pores or weekly bound particle interfaces in the LPCS-Cu coating will act as the source of pitting, which destroys the integrity of the corrosion product film and further aggravates the corrosion rate. The gap is also observed in 500 W laser-assisted LPCS coating, resulting in no significant improvement in corrosion resistance. In contrast, the 600 W and 700 W laser-assisted LPCS-Cu coatings are all dense and present excellent inter-particle bonding, which shows impermeable and excellent corrosion protection.

3.3.3 Corrosion mechanism

The corrosion behavior of the laser-assisted LPCS-Cu coatings in a neutral chloride solution mainly includes redox dissolution of Cu and material removal caused by corrosion of coating structure. The schematic diagram of the corrosion mechanism is shown in Fig. 13. After immersion of the Cu coatings in 3.5 wt.% NaCl solution, chloride ions (Cl^-) are adsorbed on the surface of coatings to form CuCl film, and CuCl will dissolve and further react to form Cu_2O film. Eventually, copper oxides and chlorides are formed on the surface. Moreover, the minimum thickness of all copper coatings is 600 μm and the porosity is less than 3%. Thus, corrosion only occurs in the surface microstructures of all Cu coatings, and the corrosion solution did not penetrate into the interface and caused corrosion

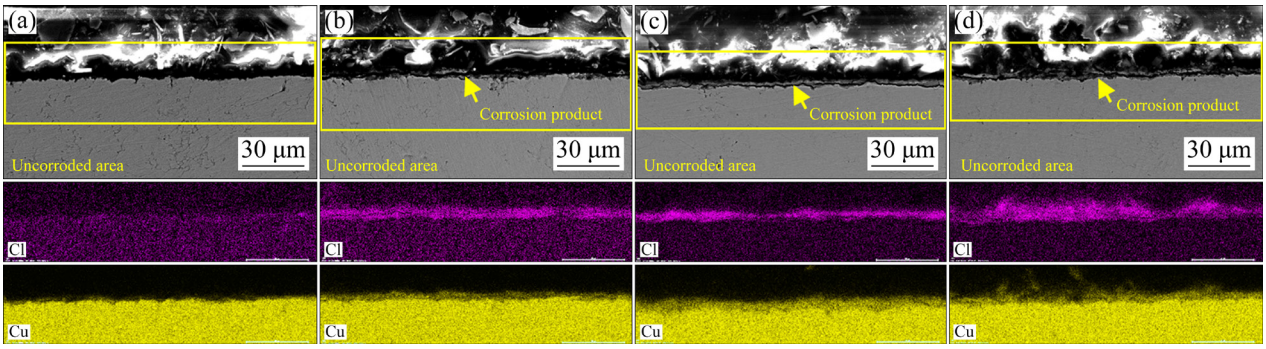

Fig. 12 Cross-sectional microstructures and EDS results of LPCS-Cu coatings assisted with different laser powers after corrosion in 3.5 wt.% NaCl solution: (a) 0 W; (b) 500 W; (c) 600 W; (d) 700 W

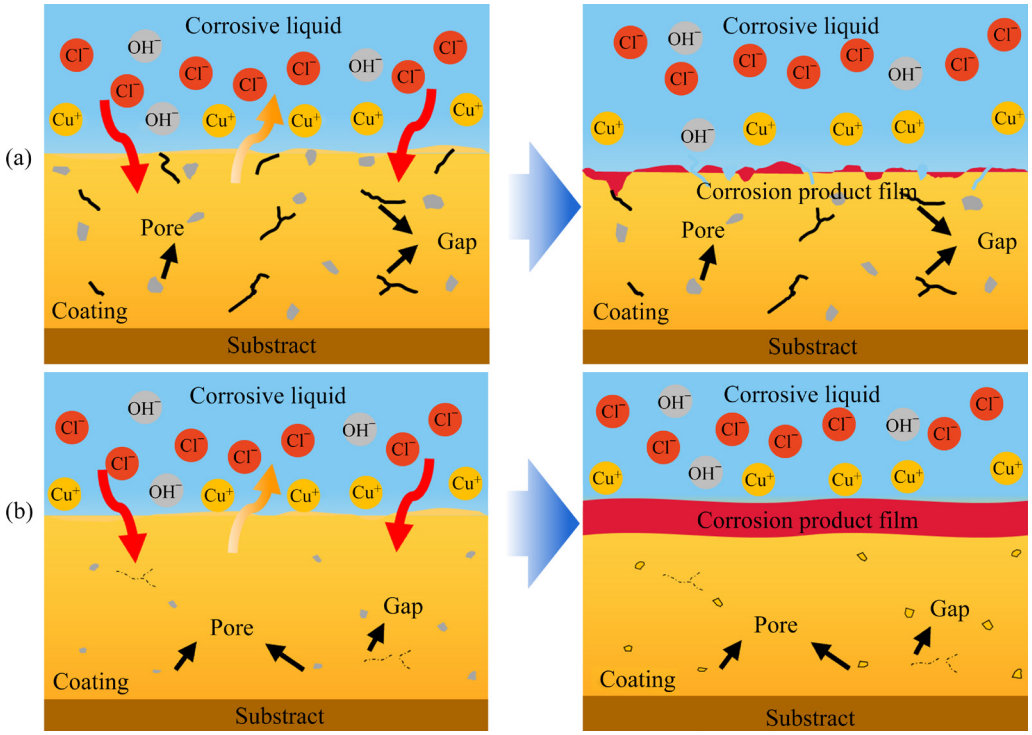

Fig. 13 Schematic diagrams of corrosion process: (a) LPCS-Cu coating; (b) Laser-assisted LPCS-Cu coating

at the interface in the electrochemical test. However, due to different structures of LPCS-Cu and laser-assisted LPCS-Cu coatings, their subsequent corrosion processes are not the same. As shown in Fig. 13(a), because of the existence of micro-pores and gaps in LPCS-Cu coating, pitting corrosion is prone to occur, and poorly bound particles are easily detached from the coating. Furthermore, it is impossible to form a continuous and dense corrosion product film on the coating surface. As shown in Fig. 13(b), because laser irradiation improves the structure compactness and bonding strength of LPCS-Cu coating, pitting in laser-assisted LPCS-Cu coating is reduced. A continuous and dense corrosion product film is formed on the surface of the laser-assisted LPCS-Cu coating, which prevents the coating from being corroded further. Therefore, high density and continuous dense corrosion product film on the surface are the key factors for good corrosion resistance of laser-assisted LPCS-Cu coatings.

4 Conclusions

(1) The laser-assisted LPCS-Cu coatings had a denser surface and a tighter interface between the coating and substrate compared to the LPCS-Cu coatings, benefiting from the simultaneous heating and softening of the deposited particles and the substrate by laser irradiation. Laser irradiation greatly reduced the porosity of LPCS-Cu coatings.

(2) The plastic deformation of the Cu particles in the laser-assisted LPCS-Cu coatings is severer than that in the LPCS-Cu coating, which possesses a more uniform microstructure and smaller grain size.

(3) The laser-assisted LPCS-Cu coatings have higher φ_{corr}, lower J_{corr} and corrosion rates than LPCS-Cu coating. The more gaps and pores are the main reasons for the poor corrosion-resistant performance of the LPCS-Cu coating because they are the fast pathways for the corrosive media to penetrate into the coating. Laser irradiation improves the coating density and intimate bonding between particles, and a continuous and dense corrosion product film composed of CuCl and Cu_2O is formed on the surface of the laser-assisted LPCS-Cu coating to block the erosion of the corrosive solution. Therefore, laser-assisted LPCS-Cu coatings exhibit better corrosion resistance than LPCS-Cu coating.

CRediT authorship contribution statement

Li-juan WU: Investigation, Characterization, Data interpretation, Visualization, Validation, Writing − Original draft, Writing − Review & editing; **Zhong-wei LIN:** Investigation, Writing − Original draft, Data curation, Visualization, Validation; **Zhun LUO:** Investigation, Validation, Writing − Original draft; **Bo LI:** Conceptualization, Methodology, Writing − Review & editing; **Jiang LIU:** Resources, Writing − Review & editing; **Qun-li ZHANG:** Supervision, Writing − Review & editing; **Jian-hua YAO:** Project administration, Funding acquisition, Conceptualization.

Declaration of competing interest

The authors declare that they have no known competing financial interests or personal relationships that could have appeared to influence the work reported in this paper.

Acknowledgments

The authors would like to appreciate financial supports from the National Natural Science Foundation of China (No. 52075495), the Natural Science Foundation of Zhejiang Province, China (No. LY22E050017), and the Fundamental Research Funds for the Provincial Universities of Zhejiang, China (No. RF-A2020009).

References

[1] HUH J H, KIM S H, CHU J H, KIM S Y, KIM J H, KWON S Y. Enhancement of seawater corrosion resistance in copper using acetone-derived graphene coating [J]. Nanoscale, 2014, 6: 4379−4386.

[2] SUO X K, ABDOLI L, LIU Y, XIA P, YANG G J, LI H. Colonization of bacteria on the surfaces of cold-sprayed copper coatings alters their electrochemical behaviors [J]. Journal of Thermal Spray Technology, 2017, 26: 687−694.

[3] QU S, DING J H, FU J, FU M W, ZHANG B C, SONG X. High-precision laser powder bed fusion processing of pure copper [J]. Additive Manufacturing, 2021, 48: 102417.

[4] SINGH S, SINGH P, SINGH H, BUDDU R K. Characterization and comparison of copper coatings developed by low pressure cold spraying and laser cladding techniques [J]. Materials Today: Proceedings, 2019, 18: 830−840.

[5] STOLTENHOFF T, BORCHERS C, GARTNER F, KREYE H. Microstructures and key properties of cold-sprayed and thermally sprayed copper coatings [J]. Surface and Coatings Technology, 2006, 200: 4947−4960.

[6] CHAMPAGNE V, HELFRITCH D. The unique abilities of cold spray deposition [J]. International Materials Reviews, 2016, 61: 437−455.

[7] SUN Wen, CHU Xin, LAN Hai-ming, HUANG Ren-zhong,

HUANG Ji-bo, XIE Ying-chun, HUANG Jian, HUANG Guo-sheng. Current implementation status of cold spray technology: A short review [J]. Journal of Thermal Spray Technology, 2022, 31: 848−865.

[8] KIM Y K, LEE K A. Effect of carrier gas species on the microstructure and compressive deformation behaviors of ultra-strong pure copper manufactured by cold spray additive manufacturing [J]. Journal of Materials Science & Technology, 2022, 97: 264−271.

[9] MORENO-MURGUIA B, MORA-GARCIA A G, CANALES-SILLER H, GIRALDO-BETANCUR A L, ESPINOSA-ARBELAEZ D G, MUÑOZ-SALDAÑA J. Influence of stand-off distance and pressure in copper coatings deposition efficiency and particle velocity [J]. Surface and Coatings Technology, 2022, 430: 127986.

[10] KIM J, BAE G, LEE C. Characteristics of kinetic sprayed Ta in terms of the deposition behavior, microstructural evolution and mechanical properties: Effect of strain-rate-dependent response of Ta at high temperature [J]. Materials Characterization, 2018, 141: 49−58.

[11] SINGH R, KONDÁS J, BAUER C, CIZEK J, MEDRICKY J, CSAKI S, ČUPERA J, PROCHÁZKA R, MELZER D, KONOPÍK P. Bulk-like ductility of cold spray additively manufactured copper in the as-sprayed state [J]. Additive Manufacturing Letters, 2022, 3: 100052.

[12] LI W B, WU H J, VERDY C, COSTIL S, LIAO H L, DENG S H. Study of low-pressure cold spray additive manufacturing: Investigation of kinematic spray parameters on deposition and properties [J]. 3D Printing and Additive Manufacturing, 2023, 10: 1260−1271.

[13] LI Zhong-sheng, WU Hu-lin, DING Xing-xing, SONG Kai-qiang, ZHANG Min, LI Li, HUANG An-wei, CONG Da-long. Effect of reinforcement particles on cold-sprayed Al-based coatings [J]. Surface Engineering, 2021, 37: 1570−1578.

[14] WINNICKI M, BASZCZUK A, JASIORSKI M, MAŁACHOWSKA A. Corrosion resistance of copper coatings deposited by cold spraying [J]. Journal of Thermal Spray Technology, 2017, 26: 1935−1946.

[15] WINNICKI M, MAŁACHOWSKA A, BASZCZUK A, RUTKOWSKA-GORCZYCA M, KUKLA D, LACHOWICZ M, AMBROZIAK A. Corrosion protection and electrical conductivity of copper coatings deposited by low-pressure cold spraying [J]. Surface and Coatings Technology, 2017, 318: 90−98.

[16] HUANG G S, MA L, XING L K, LI X B. Bonding characteristics of cold sprayed copper coating on alumina coated Q235 steel substrate [J]. Materials Science: Medziagotyra, 2021, 27: 407−415.

[17] ZHANG Zhi-chao, LIU Fu-chun, HAN En-hou, XU Long. Mechanical and corrosion properties in 3.5% NaCl solution of cold sprayed Al-based coatings [J]. Surface and Coatings Technology, 2020, 385: 125372.

[18] BRAY M, COCKBURN A, O'NEILL W. The Laser-assisted Cold Spray process and deposit characterisation [J]. Surface and Coatings Technology, 2009, 203: 2851−2857.

[19] LUPOI R, SPARKES M, COCKBURN A, O'NEILL W. High speed titanium coatings by supersonic laser deposition [J]. Materials Letters, 2011, 65: 3205−3207.

[20] JONES M, COCKBURN A, LUPOI R, SPARKES M, O'NEILL W. Solid-state manufacturing of tungsten deposits onto molybdenum substrates with supersonic laser deposition [J]. Materials Letters, 2014, 134: 295−297.

[21] OLAKANMI E O, DOYOYO M. Laser-assisted cold-sprayed corrosion- and wear-resistant coatings: A review [J]. Journal of Thermal Spray Technology, 2014, 23: 765−785.

[22] LI B, YANG L J, LI Z H, YAO J H, ZHANG Q L, CHEN Z J, DONG G, WANG L. Beneficial effects of synchronous laser irradiation on the characteristics of cold-sprayed copper coatings [J]. Journal of Thermal Spray Technology, 2015, 24: 836−847.

[23] ZHANG Q L, WU L J, ZOU H S, LI B, ZHANG G, SUN J Y, WANG J J, YAO J H. Correlation between microstructural characteristics and cavitation resistance of Stellite-6 coatings on 17-4 PH stainless steel prepared with supersonic laser deposition and laser cladding [J]. Journal of Alloys and Compounds, 2021, 860: 158417.

[24] NIKBAKHT R, COJOCARU C V, AGHASIBEIG M, IRISSOU E, KIM T S, KIM H S, JODOIN B. Cold spray and laser-assisted cold spray of CrMnCoFeNi high entropy alloy using nitrogen as the propelling gas [J]. Journal of Thermal Spray Technology, 2022, 31: 1129−1142.

[25] BUCHANAN R A, STANSBURY E E. Handbook of environmental degradation of materials [M]. 2nd ed. Oxford: William Andrew Publishing, 2012: 87−125.

[26] WEI Ying-kang, LUO Xiao-tao, CHU Xin, GE Yi, HUANG Guo-sheng, XIE Ying-chun, HUANG Ren-zhong, LI Chang-jiu. Ni coatings for corrosion protection of Mg alloys prepared by an in-situ micro-forging assisted cold spray: Effect of powder feedstock characteristics [J]. Corrosion Science, 2021, 184: 109397.

[27] MUNAGALA V N V, AKINYI V, VO P, CHROMIK R R. Influence of powder morphology and microstructure on the cold spray and mechanical properties of Ti6Al4V coatings [J]. Journal of Thermal Spray Technology, 2018, 27: 827−842.

[28] NING X J, JANG J H, KIM H J. The effects of powder properties on in-flight particle velocity and deposition process during low pressure cold spray process [J]. Applied Surface Science, 2007, 253: 7449−7455.

[29] YIN S, WANG X F, SUO X K, LIAO H L, GUO Z W, LI W Y, CODDET C. Deposition behavior of thermally softened copper particles in cold spraying [J]. Acta Materialia, 2013, 61: 5105−5118.

[30] YU M, LI W Y, WANG F F, SUO X K, LIAO H L. Effect of particle and substrate preheating on particle deformation behavior in cold spraying [J]. Surface and Coatings Technology, 2013, 220: 174−178.

[31] KOIVULUOTO H, COLEMAN A, MURRAY K , KEARNS M, VUORISTO P. High pressure cold sprayed (HPCS) and low pressure cold sprayed (LPCS) coatings prepared from OFHC Cu feedstock overview from powder characteristics to coating properties [J]. Journal of Thermal Spray Technology, 2012, 21: 1065−1075.

[32] DA SILVA F S, CINCA N, DOSTA S, CANO I G, GUILEMANY J M, CAIRES C S A, LIMA A R, SILVA C M, OLIVEIRA S L, CAIRES A R L, BENEDETTI A V. Corrosion resistance and antibacterial properties of copper

coating deposited by cold gas spray [J]. Surface and Coatings Technology, 2019, 361: 292−301.
[33] KOIVULUOTO H, LAGERBOM J, VUORISTO P. Microstructural studies of cold sprayed copper, nickel, and nickel−30% copper coatings [J]. Journal of Thermal Spray Technology, 2007, 16: 488−497.
[34] KOIVULUOTO H, MILANTI A, BOLELLI G, LATOKARTANO J, MARRA F, PULCI G, VIHINEN J, LUSVARGHI L, VUORISTO P. Structures and properties of laser-assisted cold-sprayed aluminum coatings [J]. Materials Science Forum, 2016, 879: 984−989.
[35] TARIQ N U, GYANSAH L, QIU X, JIA C N, BIN AWAIS H, ZHENG C W, DU H, WANG J Q, XIONG T Y. Achieving strength-ductility synergy in cold spray additively manufactured Al/B_4C composites through a hybrid post-deposition treatment [J]. Journal of Materials Science & Technology, 2019, 35: 1053−1063.
[36] CINCA N, DREHMANN R, DIETRICH D, GÄRTNER F, KLASSEN T, LAMPKE T, GUILEMANY J M. Mechanically induced grain refinement, recovery and recrystallization of cold-sprayed iron aluminide coatings [J]. Surface and Coatings Technology, 2019, 380: 125069.
[37] SHAO Guo-sen, GAO Yu-hang, WU Jia-yan, LIU Ping, ZHANG Ke, LI Wei, MA Feng-cang, ZHOU Hong-lei, CHEN Xiao-hong. Effect of Fe/Mn content on mechanical and corrosion properties of 90/10 copper–nickel alloy [J]. Materials and Corrosion, 2022, 73: 1085−1098.
[38] RALLS A M, DAROONPARVAR M, SIKDAR S, RAHMAN M H, MONWAR M, WATSON K, KAY C M, MENEZES P L. Tribological and corrosion behavior of high pressure cold sprayed duplex 316 L stainless steel [J]. Tribology International, 2022, 169: 107471.
[39] NGAI S, NGAI T, VOGEL F, STORY W, THOMPSON G B, BREWER L N. Saltwater corrosion behavior of cold sprayed AA7075 aluminum alloy coatings [J]. Corrosion Science, 2018, 130: 231−240.
[40] HASSANI-GANGARAJ S M, MORIDI A, GUAGLIANO M. Critical review of corrosion protection by cold spray coatings [J]. Surface Engineering, 2015, 31: 803−815.
[41] MENG X M, ZHANG J B, ZHAO J, LIANG Y L, ZHANG Y J. Influence of gas temperature on microstructure and properties of cold spray 304SS coating [J]. Journal of Materials Science & Technology, 2011, 27: 809−815.
[42] DING Ke-qiang, QU Run-ling, ZHOU Lan-jun, ZHANG Dong-yue, CHEN Jia-sheng, HE Xiang-ming, WANG Li, WANG Hui, DOU Hong-min. In situ preparation of CuCl cubic particles on the commercial copper foil: Its significant facilitation to the electrochemical performance of the commercial graphite and its unexpected photochromic behavior [J]. Journal of Alloys and Compounds, 2020, 835: 155302.
[43] RUI D, LI X B, JIA W B, LI W H, XIAO W, GUI T J. Releasing kinetics of dissolved copper and antifouling mechanism of cold sprayed copper composite coatings for submarine screen doors of ships [J]. Journal of Alloys and Compounds, 2018, 763: 525−537.

激光辅助低压冷喷涂 Cu 涂层的显微组织和腐蚀性能

吴丽娟[1,2,3]，林钟卫[1,2,3]，罗 准[1,2,3]，李 波[1,2,3]，刘 江[4]，张群莉[1,2,3]，姚建华[1,2,3]

1. 浙江工业大学 机械工程学院，杭州 310023；
2. 浙江工业大学 激光先进制造研究院，杭州 310023；
3. 浙江工业大学 高端激光制造设备协同创新中心，杭州 310023
4. 浙江热刺激光技术有限公司，台州 317500

摘 要：采用激光辅助低压冷喷涂(LPCS)方法制备 Cu 涂层，研究激光辐照对 Cu 涂层显微组织和腐蚀行为的影响。与 LPCS-Cu 涂层相比，激光辅助 LPCS-Cu 涂层更致密，涂层与基材的界面结合更好。激光辐照加大了沉积颗粒的整体塑性变形程度，使 Cu 沉积颗粒晶粒得到均匀细化。因此，激光辅助 LPCS-Cu 涂层呈更均匀的显微组织和更小的晶粒尺寸。电化学测试结果表明，激光辅助 LPCS-Cu 涂层在 3.5% NaCl (质量分数)溶液中比 LPCS-Cu 涂层具有更高的腐蚀电位、更低的腐蚀电流和腐蚀速率。主要原因是激光辐照提高了涂层致密度和颗粒之间的紧密结合，并在激光辅助 LPCS-Cu 涂层表面形成由 CuCl 和 Cu_2O 组成的连续、致密的腐蚀产物膜，以阻挡腐蚀溶液的侵蚀。

关键词：Cu 涂层；激光辐照；冷喷涂；显微组织；腐蚀性能

(Edited by Wei-ping CHEN)